

# Effect of Methyl Methacrylate/Polyhedral Oligomeric Silsesquioxane Random Copolymers in Compatibilization of Polystyrene and Poly(methyl methacrylate) Blends

Wenhua Zhang,<sup>†</sup> Bruce X. Fu,<sup>‡</sup> Y. Seo,<sup>†</sup> Eric Schrag,<sup>†</sup> B. Hsiao,<sup>‡</sup> Patrick T. Mather,<sup>§</sup> Nan-Loh Yang,<sup>||</sup> Dayi Xu,<sup>||</sup> Harald Ade,<sup>⊥</sup> Miriam Rafailovich,<sup>\*,†</sup> and Jonathan Sokolov<sup>†</sup>

Department of Materials Science and Engineering, SUNY, Stony Brook, New York 11794; Chemistry Department, SUNY, Stony Brook, New York 11794; Institute of Material Science, University of Connecticut, Storrs, Connecticut 06269; Chemistry Department, CUNY, Staten Island, New York 10314; and Department of Physics, North Carolina State University, Raleigh, North Carolina 27695

Received May 13, 2002

**ABSTRACT:** Random copolymers of methyl methacrylate with polyhedral oligomeric silsesquioxane (POSS) were synthesized and blended with PS and PMMA homopolymer thin films. The effects of the POSS on phase segregation were studied using a variety of complementary techniques. The results showed that these copolymers were efficient at compatibilizing immiscible polymer blends. Compatibilization occurred when the POSS was grafted onto the backbone and a favorable interaction existed between the POSS functional groups and the PS homopolymers. The consequences of this compatibilization were studied using a comprehensive array of characterization methods and found to be as follows: reduced domain size, increased interfacial width, and greatly improved fracture toughness. This compatibilization is due to the increased site functionality provided by the POSS molecule without the entropic penalty associated with introducing functionalities via grafting directly onto the polymer chains.

## Introduction

Polymer blends play an important role in industry since they provide a relatively inexpensive way to improve material characteristics by combining selected properties of the constituent polymers.<sup>1–3</sup> However, since the entropic contribution in the mixing free energy of large molecular weight polymers is low, even small unfavorable enthalpic interactions can cause phase segregation,<sup>4</sup> which results in poor thermal and mechanical properties as well as adhesive failure. Hence, a great deal of research has concentrated on reducing the interfacial tension between phases in order to control the average domain size and improve fracture toughness.<sup>5,6</sup>

The most common method of reducing interfacial tension has been to add copolymers with different architectures which segregate to interfaces and reduce the interfacial tension.<sup>7–9</sup> In addition, if the molecular weights are sufficiently large, entanglements form across interfaces, thereby improving adhesion. The major disadvantage of this technique is that these copolymers are often difficult to synthesize, and therefore, it is not cost efficient. Furthermore, competition from micelle production often limits the amount available for interfacial segregation thereby reducing the efficiency of the process.<sup>10,11</sup> Random copolymers, which are inexpensive, have been shown to be effective in increasing fracture toughness but ineffective in reducing interfacial tension.<sup>12,13</sup> Here we chose a different ap-

proach and explore the use of polymer/inorganic nanocomposites as alternatives to copolymers in promoting compatibility and adhesion in polymer blends.

The materials we chose are organic/inorganic nanocomposites, produced by random copolymerization of MMA monomers with polyhedral oligosilsesquioxane (POSS) functionalized with methacrylate. POSS molecules, first reported in 1946,<sup>14</sup> have a cage-like structure with a polyhedral silicon–oxygen nanostructured skeleton, as shown in Figure 1. The general formula is  $(\text{SiO}_{3/2})_n$  where  $n$  varies with the specific structure of the molecule; i.e.,  $n = 4$  for tetrahedron and  $n = 8$  for cubic structure. The major advantage of POSS copolymers is that a variety of substituents can be incorporated onto the R position of the silicon atom as shown in Figure 1, thereby providing a large number of chemical functionalities on the chain.<sup>15</sup> As we will show, these contribute only to the enthalpy of the chain without changing the entropic interactions at the interface. This is in contrast to graft copolymers, which have also been shown to be effective compatibilizers<sup>4</sup> at low grafting densities. As the number of grafts is increased, however, the large unfavorable entropy quickly overcomes enthalpic gains, and the interfacial tension actually increased,<sup>7</sup> thereby enhancing phase segregation.<sup>16</sup>

Numerous researchers<sup>17,18,19</sup> have reported that “grafting” POSS onto polymers such as polyurethanes and PMMA also increases the mechanical strength, thereby improving the overall properties of the materials. Hence POSS copolymers now show promise for various applications ranging from windshields to flame retardant polymer composites. Since these applications frequently require blending or interfacial adhesion with other polymers, it is important to understand the effect of the POSS on the miscibility of polymer blends.

<sup>†</sup> Department of Materials Science and Engineering, SUNY, Stony Brook.

<sup>‡</sup> Chemistry Department, SUNY, Stony Brook.

<sup>§</sup> University of Connecticut.

<sup>||</sup> CUNY, Staten Island.

<sup>⊥</sup> North Carolina State University.

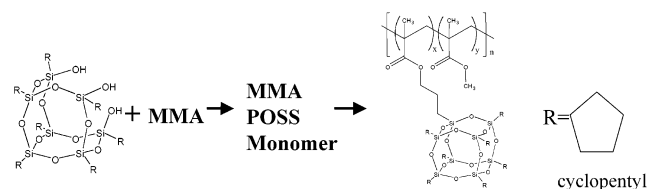


**Figure 1.** Synthesis and structure of PMMA-POSS random copolymer.

Here we study the model blend of polystyrene (PS) and poly(methyl methacrylate) (PMMA) for which monodisperse polymers are available and which has been well characterized in previous studies.<sup>20</sup> To study the effects on miscibility we used POSS molecules which have cyclopentyl in the R position. Cyclopentyl interacts more favorably with PS than PMMA, hence increasing the favorable enthalpy component. We therefore compare the effects on interfacial properties when cyclopentyl POSS is introduced as discrete molecules or grafted onto high and low  $M_w$  PMMA backbones.

Scanning probe microscopy (SPM) coupled with scanning transmission X-ray microscopy (STXM) was used to determine lateral composition and morphology. X-ray reflectivity was used to directly measure the interfacial width in bilayer films, and the asymmetric double cantilever beam (ADCM) method was used to determine the effects on interfacial fracture toughness.

## Experimental Section

**Materials and Sample Preparation.** The synthesis of POSS-containing PMMA random copolymers using conventional free radical polymerization has been described previously.<sup>23</sup> Heptacyclopentyl POSS-containing copolymers with narrow molecular weight distribution were prepared by atom transfer radical solution copolymerization, a procedure based on modifications of a reported method for bulk homo and block copolymerization.<sup>23</sup> Random copolymers of propylmethacrylate-heptacyclopentyl POSS and MMA copolymer were synthesized as follows. Methyl methacrylate (2.92 g, 29.2 mmol) and 3-(3,5,7,9,11,13,15-heptacyclopentyl)pentacyclo[9.5.1.1.3,9.1.5,15]octasiloxane-1-yl)propyl methacrylate (PMA-POSS), (0.3 g, 0.292 mmol for each mol % of POSS incorporation) were placed in a vial with a magnetic stirring bar, followed by addition of purified toluene (3.0 g) to dissolve the monomers. The solution was bubbled slowly with nitrogen for about 1 min. The catalyst  $\text{Cu}^{\text{I}}\text{Cl}$  (0.0058 g, 0.058 mmol) with PMDETA (0.048 g, 0.34 mmol) was added into the vial under  $\text{N}_2$ . After being stirred for about 20 min, the solution turned blue. Then, 8.5  $\mu\text{L}$  of initiator and ethyl 2-bromoisobutyrate (0.058 mmol) were added to the solution under  $\text{N}_2$ . The vial was capped and sealed with Parafilm. The reaction solution was stirred for 10 min at room temperature and then heated to 60  $^\circ\text{C}$  for 24 h in an oil bath. The solution was then kept at 80  $^\circ\text{C}$  for the desired polymerization time, usually 24 h or longer.

$^1\text{H}$  NMR was employed for tracking conversion of the living polymerization using chemical shifts of the methoxy protons of MMA at 3.8 ppm for monomer and 3.6 ppm for polymer. The conversion of polymerization was controlled to under 80% to avoid radical coupling reaction.

The copolymer was precipitated in methanol and then dissolved in chloroform and reprecipitated at least twice in cyclohexane to remove unreacted POSS monomer and twice in methanol to remove transition-metal catalyst. This purification procedure was continued until copolymer appeared white and no NMR signal of  $\text{CH}=\text{C}$  was observed. The molecular weight and molecular weight distribution were determined by GPC, using polystyrene as standard.

The POSS-PMMA copolymers and the homopolymers used in these experiments are summarized in Table 1. POSS particles, functionalized with cyclopentyl were purchased from

**Table 1. Summary of POSS Copolymer Used**

	$M_n$	$M_w/M_n$	wt % POSS
PMMA-POSS0	375 000	3.11	
PMMA-POSS5 <sup>a</sup> (cyclopentyl)	483 000	4.82	5.5
PMMA-POSS10 <sup>a</sup> (cyclopentyl)	409 000	2.46	8.0
PMMA-POSS15 <sup>a</sup> (cyclopentyl)	734 000	2.02	10.7
PMMA-POSS low M10	24 400	1.22	8.9
PMMA-POSS low M20	25 400	1.35	17.8

<sup>a</sup> Note: In this paper PMMA-cyclopentyl-POSS copolymers are abbreviated as PMMA-POSS5, PMMA-POSS10, and PMMA-POSS15.

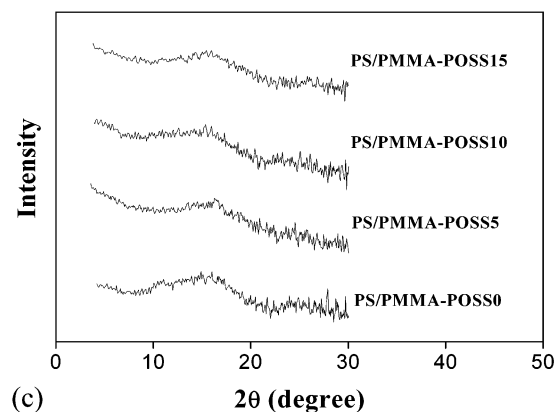
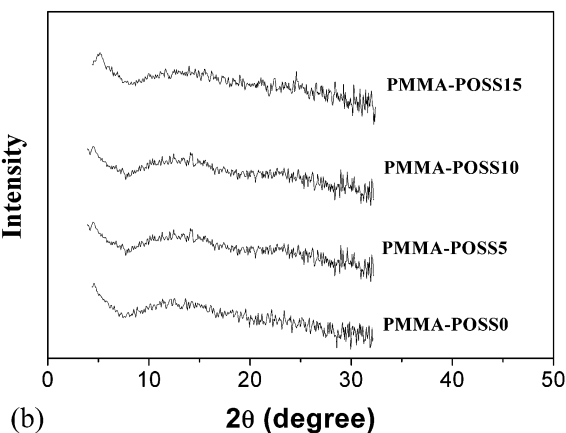
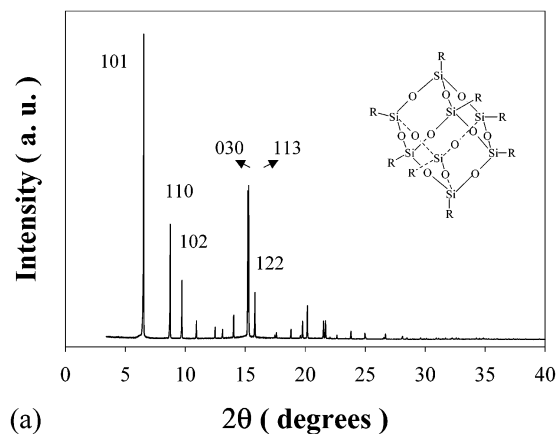


**Figure 2.** WAXD spectra of (a) pure octacyclopentyl-POSS, (b) PMMA-octacyclopentyl-POSS, and (c) PMMA-octacyclopentyl-POSS and PS blend.

Hybrid Plastics, Inc. Thin films were produced by co-dissolving functionalized POSS particles or POSS copolymers with either PS, PMMA, or both in toluene and spin casting at 2500 rpm onto HF etched Si wafers (300  $\mu\text{m}$  thick, (100) orientation, Wafer World Inc.). The film thicknesses were monitored using

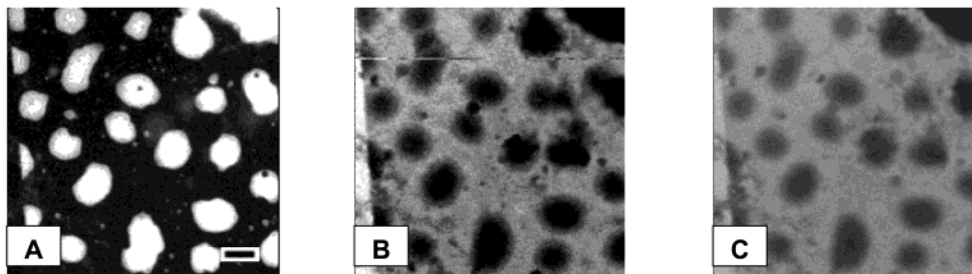


**Figure 3.** STXM images of PS/PMMA film after 24 h of annealing at 170 °C: (A) "PS" image taken at 285.2 eV; (B) "PMMA" image taken at 288.6 eV; (c) topography image taken at 280 eV. (Black bar in the image is 2  $\mu\text{m}$ .)

ellipsometry. The samples were annealed in a vacuum of  $10^{-3}$  Torr at  $T = 170$  °C for various times and then the morphology was analyzed with either scanning probe microscopy (SPM) or scanning transmission X-ray microscopy (STXM).

**X-ray Reflectivity.** The effect of POSS on the interfacial width between PS and PMMA was measured by forming bilayer samples. These were produced by spin casting the PMMA-POSS copolymer directly onto the Si wafers and then floating another film of PS on top. The thickness of the films were measured with a model Rudolph "auto EL" ellipsometer and found to range from 600 to 1100 Å. The bilayer samples were annealed for 1 h at 170 °C to allow the interface to relax. The interfacial width was then measured using X-ray reflectivity<sup>21</sup> on beamline X10B of the National Synchrotron Light Source at Brookhaven National Laboratory.

**Scanning Probe Microscopy.** The surface topography and lateral force images of the films were obtained using a Veeco/DI Dimension 3000 SPM in the contact mode with  $\text{Si}_3\text{N}_4$  tip.

**Scanning Transmission X-ray Microscopy.** The STXM samples were prepared by removing the PS/PMMA films from the Si substrates in KOH solution at 80 °C and floating onto TEM grids. Experiments were carried out with the scanning transmission X-ray microscopy on beamline X1A (X1A-STXM) of the National Synchrotron Light Source at Brookhaven National Laboratory. The samples were imaged under He atmosphere to minimize absorption of the analyzing beam. Details about the instrument are described by Jacobsen et al.,<sup>24</sup> and its applications to polymers were reviewed by Ade.<sup>25</sup> The lateral resolution in these experiments was better than 100 nm.

**Fracture Toughness.** The effect of the fracture toughness at the PS/PMMA interface was investigated using the asymmetric double cantilever method.<sup>6,26</sup> Plates of polydispersed PS and PMMA with dimensions of 1 cm  $\times$  7 cm  $\times$  17 mm were made by compression molding at 160 °C. A thin film of the PMMA-POSS copolymer, approximately 100 nm thick, was spun cast from solution onto the PS plate. The two plates were then joined at 165 °C for 10 min. A razor blade was inserted at the interface at a constant speed of 10  $\mu\text{m/s}$ , and the crack length was recorded using optical microscopy. Each data point represents the average of three samples with 15 data points on each sample. The crack length is converted to interfacial fracture toughness  $G_c$  using the following relations by Kanninen and Creton<sup>6</sup>

$$G_c = \frac{3u^2ED^3}{8a^4[1 + 0.64(D/a)]^4} \quad (1)$$

Here  $u$  is the wedge thickness or the thickness of the razor blade,  $E = 3.0 \times 10^9$  Pa is Young's modulus of PS in the top layer,  $D$  is the thickness of top layer, and  $a$  is the crack length.

**WAXD.** Wide-angle X-ray diffraction (WAXD) measurements were carried out at the Advanced Polymers beamline, X27C, National Synchrotron Light Source (NSLS), Brookhaven National Laboratory (BNL). The wavelength used was 0.1307 nm, and the beam size was about 0.4 mm in diameter at the sample position. A Fuji imaging plate was used to detect WAXD images. The sample-to-detector distance for WAXD was 140 mm and the WAXD profiles were calibrated by a silicon standard.

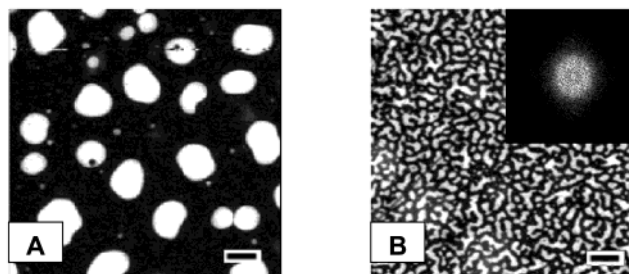


**Figure 4.** STXM images of films after 24 h of annealing at 170 °C: (A) PS/PMMA with 2% (w) cyclopentyl-POSS particle; (B) PS/PMMA with 10% cyclopentyl-POSS-PMMA copolymer. (Black bars in the image are 2  $\mu\text{m}$  in length; both images are "PS" images which were taken at 285.2 eV.)

## Results and Discussions

**WAXD Characterization of PMMA-POSS.** The WAXD spectra of a pure octacyclopentyl-POSS sample is shown in Figure 2a where we can see that the octacyclohexyl-POSS (1,3,5,7,9,11,13,15-octacyclohexyl-pentacyclo[9.5.1.13.9.15,15.17,13]octasiloxane) has a rhombohedral cell with  $a = 11.57$  Å and  $\theta = 95.5^\circ$ . The WAXD spectra of the pure copolymer is shown in Figure 2b for POSS fractions of 5, 10, and 15%. From the figure we can clearly see that the peaks corresponding to crystalline POSS are gone and the samples are amorphous. This is in contrast to the data reported by Fu et al.<sup>18</sup> for heptacyclopentyl POSS-polyurethane (PU) random copolymers where POSS crystalline peaks appeared at a volume fraction of 10%. In the case of PU, the POSS crystallinity was believed to be induced by crystallization of the hard segments in the urethane copolymer. In our system, the PMMA is amorphous and no ordering of the backbone occurs. Hence the spectra indicate that POSS is well dispersed within the matrix and no agglomerates large enough to crystallize exist. Lack of crystallinity is also observed in symmetric blends of the PMMA copolymer and polystyrene.

**Scanning Transmission X-ray Microscopy (STXM).** The STXM images of films in a series of PS ( $M_w = 65\text{K}$ ) and PMMA ( $M_w = 35\text{K}$ ) symmetric blends, annealed for 24 h at 170 °C, are shown in Figure 3. In Figure 3a, we see the images of the film without POSS. Here the phase segregated morphology is similar to that previously reported by Ade et al.<sup>27</sup> Parts a and b of Figure 3 show the intensities obtained by scanning at 285.2 and 288.6 eV, where the bright areas correspond to a maximum in PS or PMMA absorption, respectively. From the figures we can then see that PMMA wets the silicon substrate while PS dewets the PMMA layer. In Figure 4, we show the morphologies obtained from the PS intensity spectra, when POSS is added in various forms to the blend prior to annealing. In Figure 4a, we see

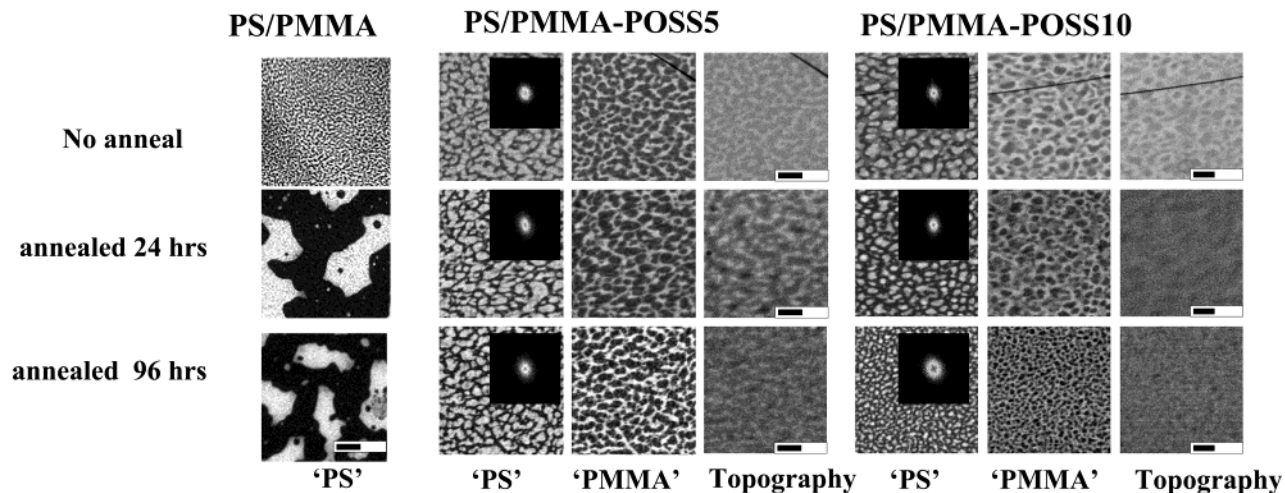


**Figure 5.** STXM images of films after 24 and 96 h of annealing at 170 °C, respectively. (Black bars are 2  $\mu\text{m}$  in length.)

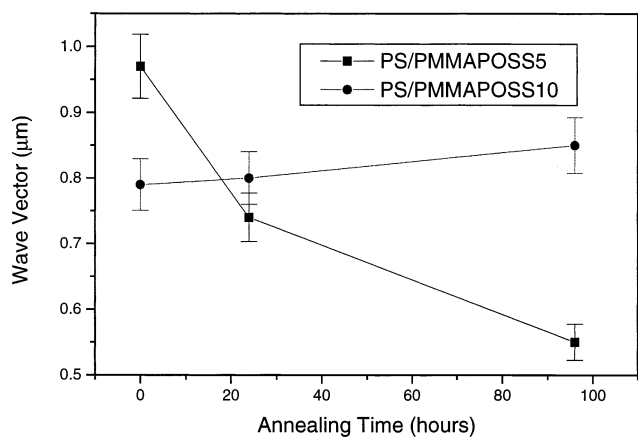


**Figure 6.** Wave vector of PS/PMMAPOSS(50/50) blend thin film as a function of annealing time.

the morphology when 2 wt % octacyclopentyl-POSS molecules are added to the blend; this amount of POSS is the same as that introduced by adding the 10% PMMA-heptacyclopentyl-POSS15 copolymer. In this case, it is apparent that the POSS has no effect on the phase-segregated structures. In Figure 4b, we show the morphology obtained when adding 10% PMMA-heptacyclopentyl-POSS15. Here we see that a bicontinuous microemulsion structure with a well-defined wave vector (see FFT in the inset) has formed, indicating that the interfacial tension between the phases has been reduced. A similar microemulsion structure was previously reported by Gersappe et al.,<sup>21</sup> as formed by confinement of diblock copolymers at the phase interfaces between PS and PMMA.

To determine whether in this case the microemulsion phase was an equilibrium structure of the blend or an artifact associated with the spin-casting process, we studied the evolution of the microstructure as a function of time. The images are shown in Figure 5 for PMMA-heptacyclopentyl-POSS5 and PMMA-heptacyclopentyl-POSS10 added to the blends. For comparison purposes, we also show the spectra for the PMMA/PS blend annealed under the same conditions. From the figure, we can see that the morphologies of the as cast films are nearly the same regardless of the addition of POSS copolymer. Here the morphology is a nonequilibrium structure which may be a function of spinning speed, evaporation rate, and solvent/substrate interac-

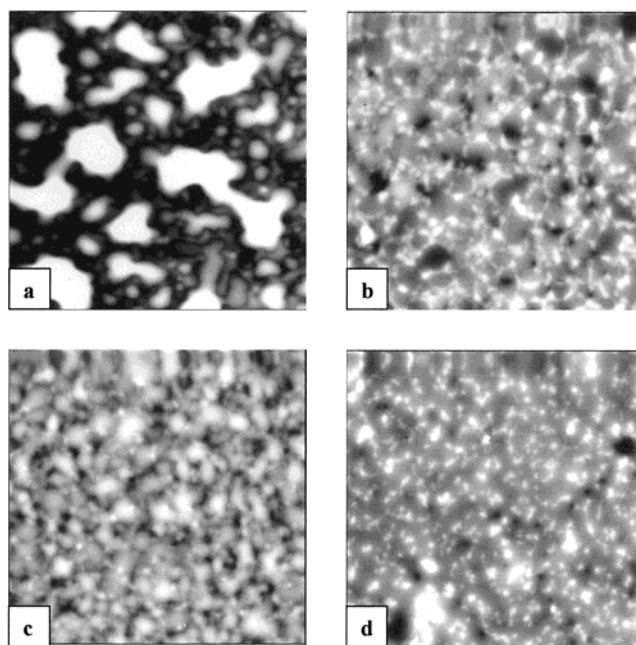


**Figure 7.** SPM images of films after 96 h of annealing at 170 °C: (a) PS/PMMA-POSS0; (b) PS/PMMA-POSS5; (c) PS/PMMA-POSS10; (d) PS/PMMA-POSS15. (All images are 25  $\mu\text{m}$  by 25  $\mu\text{m}$  scans.)

tions. Large differences become apparent after annealing for 24 h. In the case of the pure blend, the PS and PMMA form completely phase-segregated structures, while a bicontinuous structure persists in the blends with copolymers. With further annealing, the phase segregation in the pure film becomes more pronounced. In the blends with the POSS copolymers, the bicontinuous structures appear stable with time. In Figure 6, we plot the peak wave vector of the microemulsion obtained from the fast Fourier transform analysis spectra as a function of annealing time. From the figure we can see that the wave vector rapidly decreases with annealing time for the heptacyclopentyl-POSS10 sample and generally remains constant for the heptacyclopentyl-POSS5 sample. The fact that refinement is observed in the sample with the *larger* POSS fraction indicates that the addition of POSS itself does not reduce the dynamics to the point where phase pinning within the observation time occurs. Furthermore, the fact that the wave vector

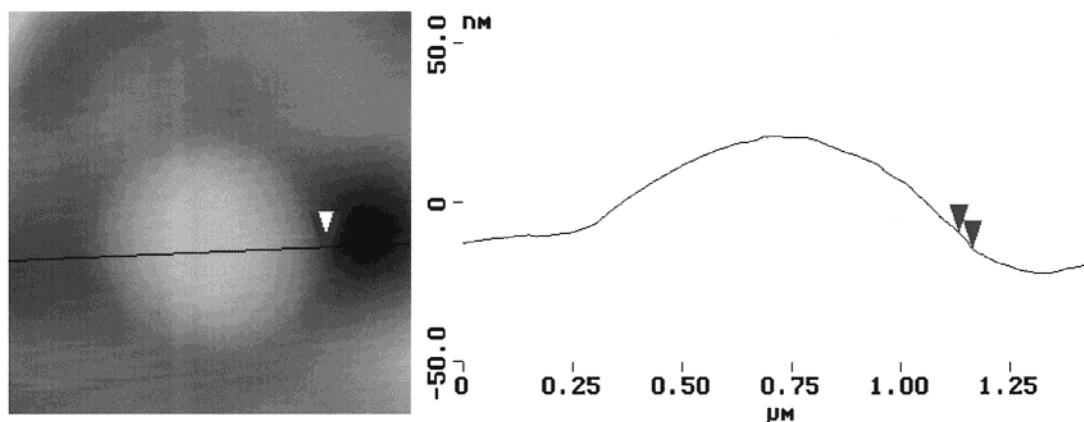


**Figure 8.** Typical contact angle measurement of a PS-PMMA blend after sample annealing at 170 °C for 24 h.

for the heptacyclopentyl-POSS10 sample increases indicates that the POSS induces compatibilization, and the equilibrium structure is more phase mixed than the initial as cast morphology. The lack of change in the wave vector of heptacyclopentyl-POSS5 films may therefore be interpreted as having achieved the equilibrium structure, rather than the lack of chain mobility. This also implies that heptacyclopentyl-POSS5 is a less efficient compatibilizer than heptacyclopentyl-POSS10, and hence, equilibrium is reached with larger domain structures.

To quantify the reduction of the interfacial tension as a function of POSS concentration, we measured the interfacial width directly using X-ray reflectivity and the interfacial tension from the Young-Neumann contact angles using scanning probe microscopy. This method has been shown to produce accurate results for PS/PMMA blends, which compared favorably with values deduced from pendant drop measurements<sup>29</sup> and theoretical calculations.<sup>30,31</sup> The results are reported below.

**Scanning Probe Microscopy.** To obtain the contact angles, two types of blends were studied. In the first case we spun cast films containing 50 wt % percent PS ( $M_w = 123K$ ) and 50% PMMA-POSS $X$  copolymer. The films were annealed for 96 h at 170 °C in a vacuum and scanned. The topographical images are shown in Figure 7. From the figure we can see that for  $X = 0$  large phase separation is observed, in agreement with the STXM images. Similarly, phase segregation occurs when octacyclopentyl-POSS molecules are added. Much smaller domain structures are immediately apparent with the grafting of as little as 5% POSS onto the PMMA backbone. The contact angles were measured in each case using cross-sectional analyses shown in Figure 8. The films were then washed in cyclohexane where we confirmed that the Newman contact angle was negligible, as previously shown by Slep<sup>32</sup> for thin film blends. The interfacial tension in this case can be directly obtained from Young's contact angle relationship

$$\gamma_{PMMA} = \gamma_{PS} \cos\theta + \gamma_{PMMA/PS} \quad (2)$$

where  $\gamma_{PS} = 29.9$  mN/m and  $\gamma_{PMMA} = 31.1$  mN/m.<sup>30</sup>

The results are plotted in Figure 9, where we see that the interfacial tension decreases by 20% or more with the grafting of little as 10% cyclopentyl-POSS onto the PMMA backbone. Addition of discrete POSS molecules on the other hand has no effect on the surface tension. On the basis of these data, we can postulate the

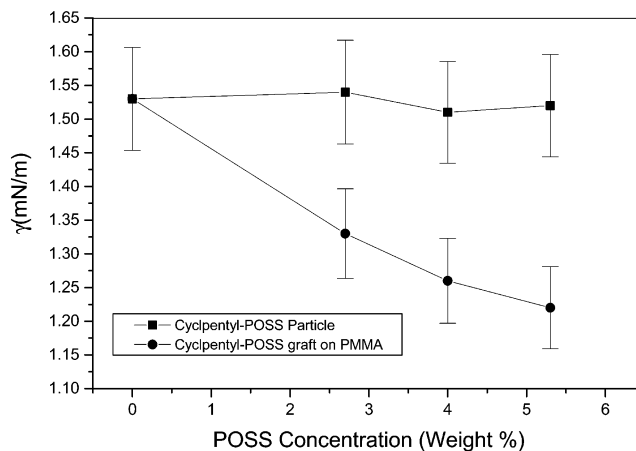


**Figure 9.** Interfacial tension calculated from observed contact angles as a function of POSS concentrations. Note that the POSS can be either grafted onto the PMMA backbone (dot) or introduced as unbound particles (squares).

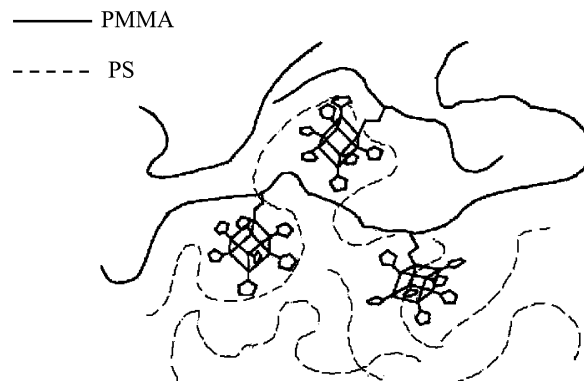


**Figure 10.** Schematic of PMMA (solid) and PS (dashed) chains in a blend when functionalized POSS is grafted onto the PMMA chains. In this case, the functional groups (cyclopentyl) interact more favorably with the PS than the PMMA monomers.

qualitative model shown in Figure 10. PS and PMMA are immiscible for the molecular weights used here. When POSS is grafted onto the PMMA, the POSS functionalities can interact separately with the PS homopolymers. If the interactions are favorable and sufficient functional groups are present on the chain, the unfavorable interactions between the PS and PMMA monomers can be overcome and commingling can result between the chains. Conversely, if the interactions with the R group are unfavorable, phase segregation of

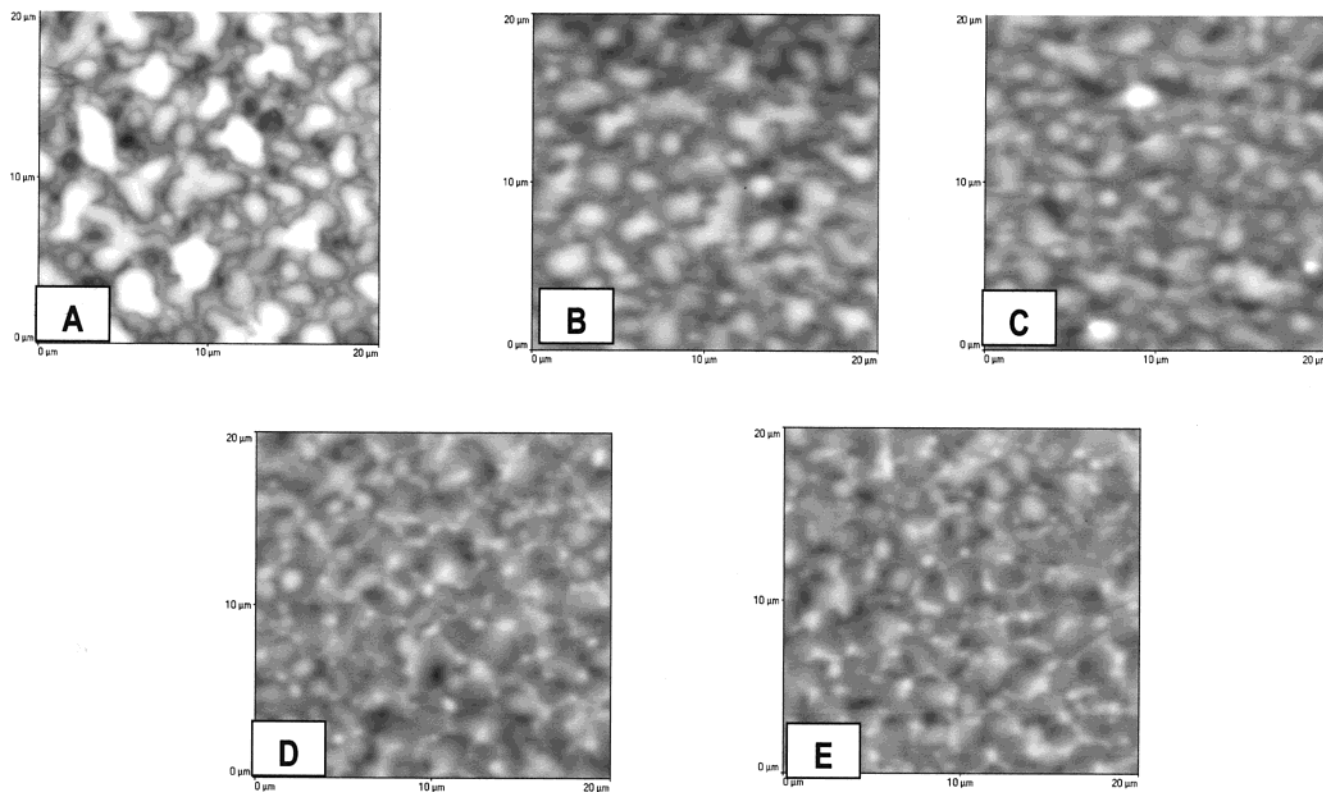


**Figure 11.** SPM images of films after 96 h of annealing at 170 °C: (A) PS/PMMA; (B) PS/PMMA with 5% PMMA-POSS15; (C) PS/PMMA with 10% PMMA-POSS15; (D) PS/PMMA with 15% PMMA-POSS15; (E) PS/PMMA with 20% PMMA-POSS15. (All images are 20  $\mu\text{m}$  by 20  $\mu\text{m}$  scans.)

the polymers may even be slightly enhanced. Hence, for reduction of interfacial tension, it is important for the POSS molecules to be attached to the backbone. Otherwise, since the interaction between particles is always more favorable than that of at least one of the components, particle aggregation will occur and the polymer phase separation will not be affected.

The POSS copolymer in essence behaves as a graft copolymer. The major difference is that the POSS molecules allow for grafting many favorable functionalities without the entropic penalty associated with increasing the number of grafts on a polymer backbone. From Figure 9, we see that the interfacial tension decreases with increasing number of POSS grafts. This in contrast to a similar curve presented by Gersappe in ref 7 where the interfacial tension increases with the number of grafts.

To further probe the compatibilization mechanisms and observe whether the copolymers were interfacially active, PS ( $M_w = 123\text{K}$ ) and PMMA ( $M_w = 35\text{K}$ ) blend films were formed where small amounts of the PMMA-POSS15 copolymer was added. The SPM images of films annealed for 96 h at 170 °C with different volume fractions of the graft copolymers are shown in Figure 11. From the figure, we see that the maximum gradient in the degree of compatibilization occurs when only 5% copolymer is added. The interfacial tension is plotted as a function of POSS copolymer concentration in Figure 12 for different fractions of POSS grafts. From the figure, we see that in all cases a large effect occurs with only 10% added graft copolymer and decreases more gradually with increasing copolymer concentration. Clearly the asymptotic value for this graph would correspond to the data shown in Figure 7, where only graft copolymers were mixed with the PS phase. This

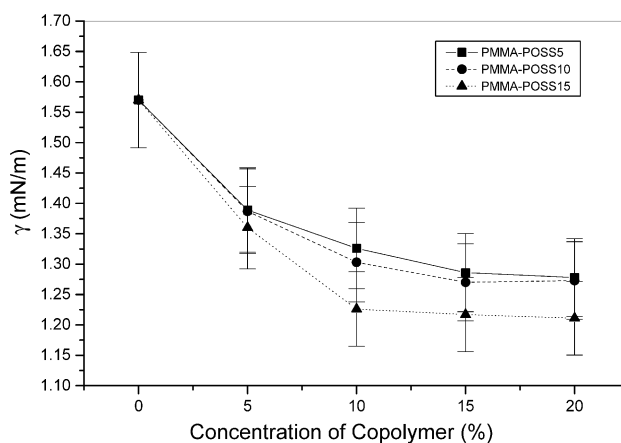


**Figure 12.** Interfacial tension calculated from observed contact angles as a function of POSS copolymer concentrations in PS-PMMA blend.

large degree of compatibilization at small volume fractions of copolymer indicates that the copolymer is interfacially active. This can be visualized in Figure 13, where we show a high resolution scan of the image in Figure 11 with 10% copolymer. In Figure 13a, we show the topography of the film after the PS phase was extracted with cyclohexane. The image is very similar to Figure 4 where we identified the PS phase using STXM. In Figure 13b, we show the lateral force scan corresponding to the topographical image. In the inset we show an expanded view of the interface left by the PS phase. A similar set of scans of a PS/PMMA phase segregated sample without the POSS copolymer is shown in parts c and d of Figure 13. Note that the segregation here is on a much larger scale. Comparing the expanded figures, we see a rim around the perimeter

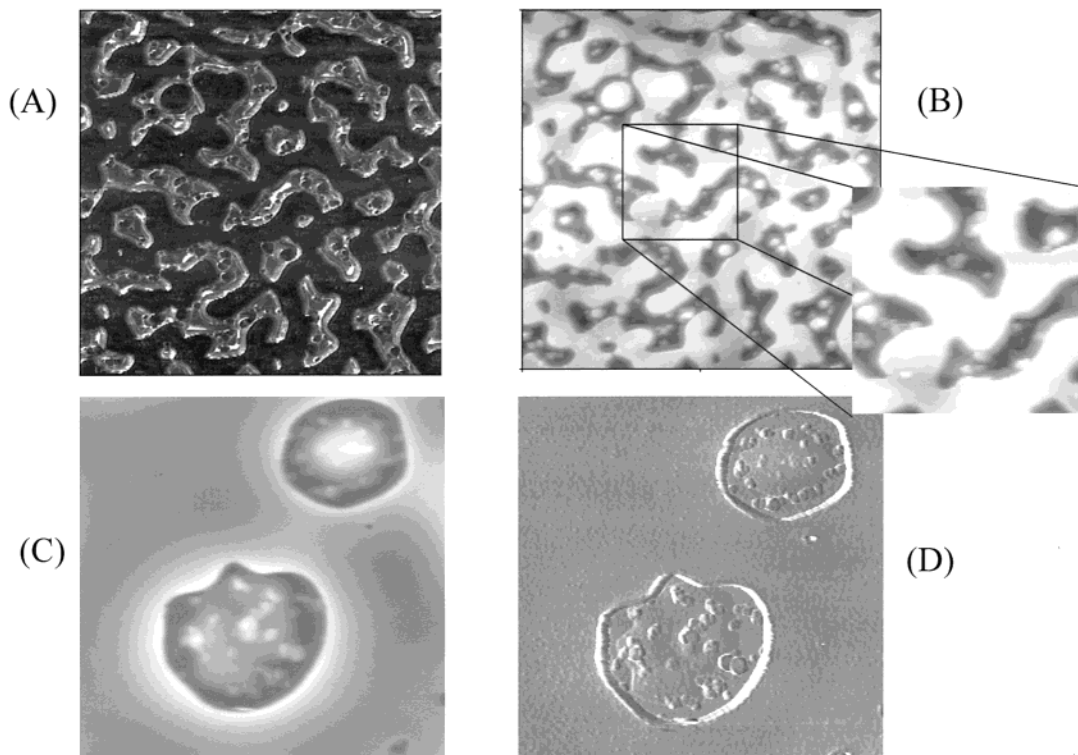


**Figure 13.** SPM images after selectively dissolving the PS phase with cyclohexane: (A) topography of PS/PMMA blend with 10% PMMA-POSS15; (B) friction of PS/PMMA blend with 10% PMMA-POSS15; (C) topography of PS/PMMA blend; (D) friction of PS/PMMA blend. Images are  $5 \mu\text{m}$  by  $5 \mu\text{m}$  scans.

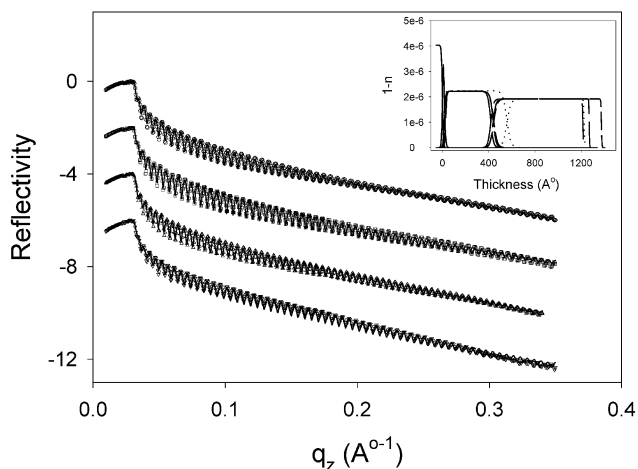


**Figure 14.** Reflectivity of PS/PMMAPOSS bilayer samples. From top to bottom: PS/PMMAPOSS0, PS/PMMAPOSS5, PS/PMMAPOSS10, and PS/PMMAPOSS15. (Inset: Scattering length density used to fit the reflectivity profiles.)

of the former PS domains only in the samples containing POSS. Since the copolymer is mostly PMMA, no direct friction contrast should be observed. On the other hand, in blends, when the copolymer is effective at compatibilization, as shown in the schematic in Figure 10, a layer of PS becomes bound to the PMMA copolymers at the interface which is not easily removed by simply rinsing with solvent. A similar effect was also shown for block copolymers in ref 20, where similar lateral force and STXM contrast were observed.

**X-ray Reflectivity.** The decreased interfacial tension should also manifest itself as an increase in the interfacial width between POSS-PMMA copolymers and PS homopolymer. Films approximately  $500 \text{ \AA}$  thick of PMMA-POSS $X$  were spun cast directly on Si wafers.

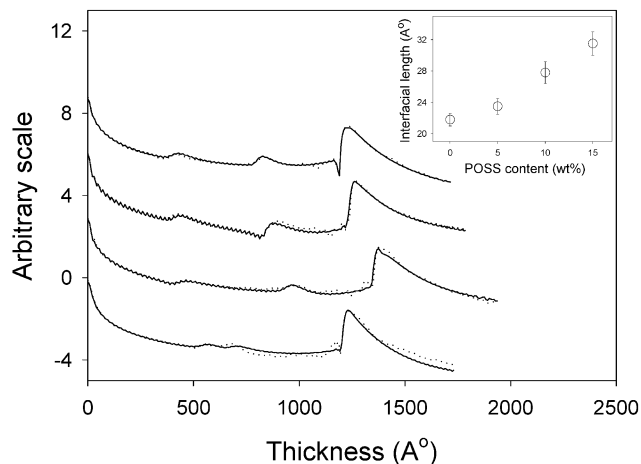


**Figure 15.** Fourier transforms of Figure 14. From top to bottom: PS/PMMAPOSS0, PS/PMMAPOSS5, PS/PMMAPOSS10, and PS/PMMAPOSS15. (Inset: interfacial width vs POSS content).

The PS films were then floated on top. The films were annealed for 1 h at  $170 \text{ }^\circ\text{C}$ . The reflectivity data, plotted as log intensity vs momentum transfer vector,  $q_z$ , are plotted in Figure 14. The solid lines are fit to the data assuming the model shown in the inset. The contrast between PMMA and PS is relatively small; hence, it is easier to analyze the Fourier transform of the data, as shown in Figure 15. This method of analysis has previously been reported<sup>28,33,34</sup> where it was shown to be more accurate than neutron reflectivity for certain polymer blends where sufficient X-ray contrast between components was present. The solid lines are fits to the data where the peak positions correspond to the thickness of the two films and the amplitude of the peaks are a measure of the interfacial width. Here the interfacial width is a combination of both interpenetra-

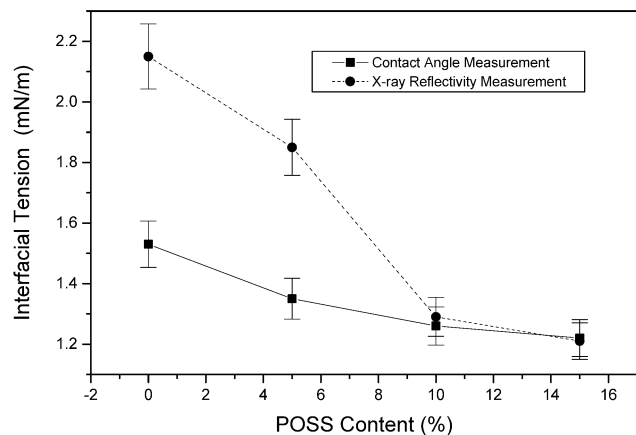


**Figure 16.** Interfacial tensions between PS and PMMA–POSS copolymer as a function of POSS content as measured by contact angle and X-ray reflectivity.

**Table 2.** PS–PMMA–POSS Copolymer Interfacial Tension

contact angle (deg)	$\gamma^{\text{contact angle}}$ (mN/m)	$\sigma^{\text{X-ray}}$ (nm)	$\gamma^{\text{X-ray}}$ (mN/m)
9.2	1.58	2.1	2.15
5.8	1.35	2.3	1.85
4.4	1.29	2.8	1.29
2.3	1.22	3.0	1.21

tion and capillary fluctuations. Both effects are a function of the interfacial tension between the layers,  $\gamma$ . The interfacial width,  $\sigma$ , can be calculated from the relationship<sup>28,33,34</sup>

$$\sigma = \left[ \frac{(a^2 \rho K_B T)^2}{18\pi\gamma^2} + \frac{K_B T}{4\pi\gamma} \ln \left( \frac{q_{\text{max}}^2}{q_{\text{coh}}^2 + q_{\text{min}}^2} \right) \right]^{1/2} \quad (3)$$

where  $a \approx 0.67$  nm and  $1/\rho \approx 0.174$  nm<sup>3</sup> is the monomer volume, and  $q_{\text{max}} = 2\pi/\sigma_{\text{intr}}$  is determined by the intrinsic roughness  $\sigma_{\text{intr}}$ . In a thin film system the lower

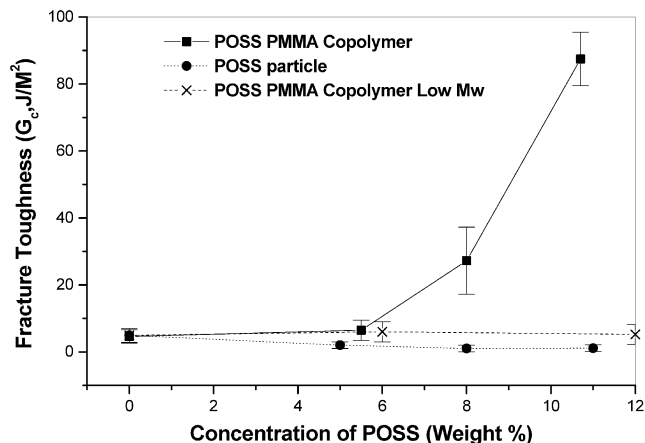


**Figure 17.** Fracture toughness of PS/PMMA interfaces reinforced with either PMMA–POSS copolymer or POSS particles.

cutoff,  $q_{\text{min}}$ , is determined by van der Waals interaction between both polymers and the substrate, set by the effective Hamaker constant  $A_{\text{eff}}$ ,  $q_{\text{min}}^2 = A_{\text{eff}}/(2\pi\gamma d^4)$ , where  $A_{\text{eff}} \approx 2 \times 10^{-20}$  J and  $d$  is the thickness of the top layer. Finally,  $q_{\text{coh}}$  is the finite coherence length of the X-ray photons, on the order of  $1.25 \times 10^{-4}$  nm<sup>-1</sup>. The results are summarized in Table 2 where we compare the interfacial tension calculated from eq 3, as well as from the Young's contact angle in eq 2 above. The values for the interfacial tension obtained by the two methods are plotted as a function of POSS content in Figure 16. From the figure, we see that both techniques show a significant decrease in interfacial tension with increasing POSS fraction.  $\gamma^{\text{X-ray}} \approx \gamma^{\text{cont}}$  for POSS fraction greater than 10%. For low POSS content,  $\gamma^{\text{X-ray}}$  is somewhat larger than  $\gamma^{\text{cont}}$  and is consistent with  $\gamma = 2.0$  mN/m previously measured by Koberstein<sup>35</sup> for PS/PMMA using the pendant drop technique. This discrepancy may be due to the fact that, as shown by Liu et al.,<sup>36</sup> the contact line is distorted at the edge of

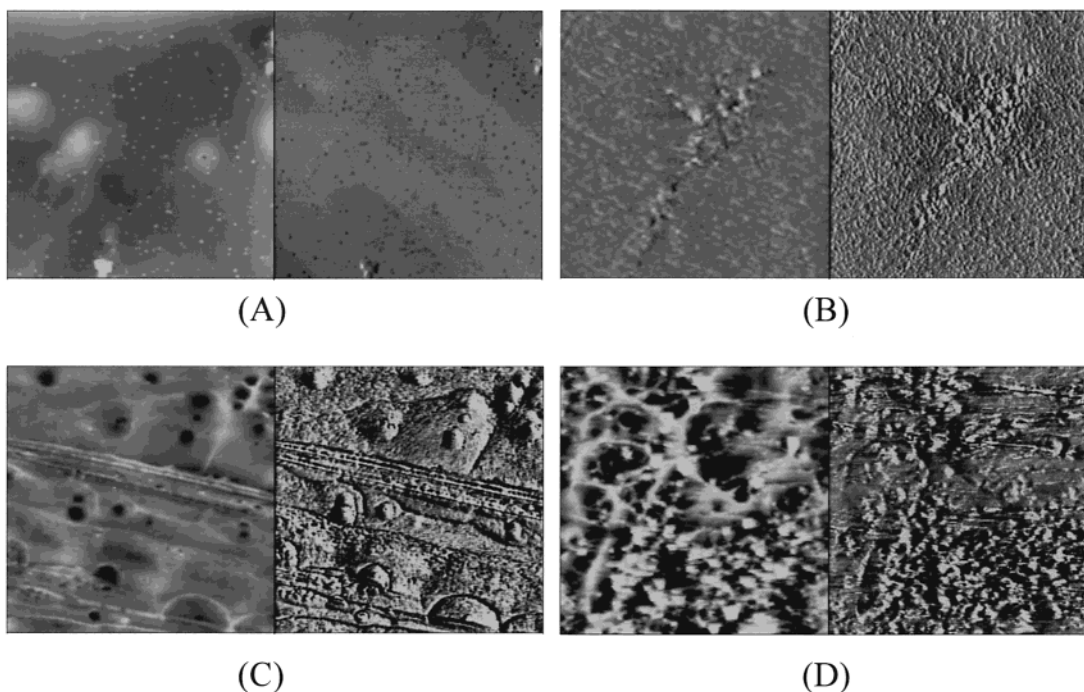


**Figure 18.** SPM images of the topography (left) and lateral force (right) of fractured PS surfaces reinforced with PMMA–POSS15: (A) PMMA–POSS0; (B) PMMA–POSS5; (C) PMMA–POSS10; (D) PMMA–POSS15

the droplet due to elastic deformation of the substrate when the contact angle is large.

**Fracture Toughness.** In addition to promoting compatibility, changing the interfacial structure also affects the adhesion between two homopolymers. Brown and others<sup>6,13</sup> have shown that random copolymers of PS and PMMA, when placed at the interface, were effective at increasing the fracture toughness between the two materials. Here we molded slabs of polydisperse PS ( $M_w = 280K$ ) and PMMA ( $M_w = 120K$ ) and spun cast a film, 200 nm thick, of PMMA–POSS copolymers, onto the PS slab. The slabs were then joined for 10 min at 160 °C and the fracture toughness tested using the asymmetric double cantilever beam test method. The fracture toughness is plotted as a function of POSS content in the copolymer in Figure 17. From the figure we can see, that as previously reported by others<sup>6</sup> the interfacial toughness between the bare PS/PMMA interfaces is very weak,  $G_c \sim 15 \text{ J/m}^2$ . The addition of 5% cyclopentyl POSS increases  $G_c$  slightly. Increasing the c-POSS content further to 8% more than doubles the fracture to  $G_c \sim 40 \text{ J/m}^2$ . Addition of copolymer with 11% POSS increases  $G_c$  by an order of magnitude to  $G_c \sim 100 \text{ J/m}^2$ , which is a value comparable to that obtained by Brown et al. using random copolymers. In the figure, we also show the fracture toughness obtained when low molecule weight ( $M_w = 24K$ ) cyclopentyl–POSS copolymer is added to the interface. From the figure, we can see that the fracture toughness does not increase even when 12% POSS is grafted onto the copolymer. Similarly, no enhancement of the interfacial strength is obtained when discrete POSS molecules are added to the interface. In Figure 18, we show SPM images of the fractured PS slab surface enhanced by PMMA–POSS0 to PMMA–POSS15. Here we see that the topographical roughness, as well as interfacial friction, increases with increasing cyclopentyl POSS–PMMA fraction. The increased friction is indicative of local plastic deformation which occurs when an interface fracture is accompanied by chain extension, crazing, and scission.

These results are also consistent with our model shown in Figure 10. The cyclopentyl–POSS grafts prefer the PS phase and drag the PMMA backbone along with them. This produces entanglements across the interface, which enhances the fracture toughness. It is reasonable to assume that the number of entanglements should increase with the concentration of POSS functionalities on the PMMA backbone, accounting for the increased fracture toughness. Hence for large values of POSS content, the crack propagates at the interface via chain scission, as observed in the SPM scans of the interface. Positioning of discrete POSS molecules at the interface does not affect fracture toughness, since they simply migrate into the PS phase without entangling in the PMMA phase. Finally, the addition of low molecular weight PMMA–POSS copolymer does not result in an increase of  $G_c$  since the backbone is short and does not allow for sufficient entanglements across the interface, which implies that a certain length of the POSS–copolymer compatibilizer is needed to show a significant effect on fracture toughness.

## Conclusions

In conclusion, we have shown that random copolymers with functionalized POSS groups can be very efficient at compatibilizing immiscible polymer blends. This com-

patibilization is due to the increased site functionality provided by the POSS molecule without the entropic penalty associated with functionalities grafted directly onto the polymer chains. Compatibilization only occurs if the POSS is grafted onto the backbone of one of the polymers. The consequences of this compatibilization were found to be as follows: reduced domain size, increased interfacial width, and greatly improved fracture toughness between immiscible polymers. The results shown in this paper are of a general nature and can be applied to other polymer blends where POSS molecules can be modified with functional groups that interact favorably with one of the components.

**Acknowledgment.** This work is supported in part by the NSF-MRSEC program. P.T.M. acknowledges support of AFOSR under Grant F49620-00-1-0100.

## Note Added after ASAP Posting

This article was released ASAP on 8/10/2002. A revised version was posted on 09/11/2002 to reflect additional changes.

## References and Notes

- (1) Ton-That, C.; Shard, A. G.; Daley, R.; Bradly, R. H. *Macromolecules* **2000**, *33*, 8453–8459.
- (2) Patnaik, S. S.; Pachter, R. *Polymer* **2002**, *43*, 415–424.
- (3) Karim, A.; Slaweki, T. M.; Kumar, S. K.; Douglas, J. F.; Satija, S. K.; Han, C. C.; Russell, T. P.; Liu, Y.; Overney, R.; Sokolov, J. C.; Rafailovich, M. H. *Macromolecules* **1998**, *31*, 857–862.
- (4) Gersappe, D.; Irvine, D.; Balaza, A. C.; Liu, Y.; Sokolov, J.; Rafailovich, M.; Schwarz, S. Peiffer, D. G. *Science* **1994**, *1072*–1074.
- (5) Lyatskaya, Y.; Balazs, A. C. *Macromolecules* **1996**, *29*, 7581–7587.
- (6) Dai, C.; Osuji, C. O.; Jandt, K. D.; Dair, B. J.; Ober, C. K.; Kramer, E. J.; Hui, C. *Macromolecules* **1997**, *30*, 6727–6736.
- (7) Lyatskaya, Y.; Gersappe, D.; Gross, N. A.; Balazs, A. C. *J. Phys. Chem.* **1996**, *100*, 1449–1458.
- (8) Janert, P. K.; Schick, M. *Macromolecules* **1997**, *30*, 137–144.
- (9) Ko, M. J.; Kim, S. H.; Jo, W. H. *Polymer* **2000**, *41*, 6387–6394.
- (10) Paul, D. R. In *Polymer Blends*; Paul, D. R., Newman, S., Eds.; Academic Press: New York, 1978; Vol. 2, p 35.
- (11) Datta, S. In *Polymeric Compatibilizers: Uses and Benefits in Polymer Blends*; Datta, S., Lohse, D. J., Eds.; Hanser/Gardner Publications: New York, 1996; 15 pp.
- (12) Lee, M. S.; Lodge, T. P.; Macosko, C. W. *J. Polym. Sci.: Part B: Polym. Phys.* **1997**, *35*, 2835–2842.
- (13) Kulasekera, R.; Kaiser, H.; Ankner, J. F.; Russell, T. P.; Brown, H. R.; Hawker, C. J.; Mayes, A. M. *Macromolecules* **1996**, *29*, 5483–5496.
- (14) Scott, D. W. *J. Am. Chem. Soc.* **1946**, *68*, 356–358.
- (15) Fu, B. X.; Hsiao, B. S.; Pagola, S.; Stephens, P.; White, H.; Rafailovich, M.; Sokolov, J.; Mather, P. T.; Jeon, H. G.; Phillips, S.; Lichtenhan, J.; Schwab, J. *Polymer* **2001**, *42*, 599–611.
- (16) Ge, S.; Guo, L.; Rafailovich, M.; Sokolov, J.; Overney, R.; Buenviajje, C.; Peiffer, D.; Schwarz, S. *Langmuir* **2001**, *17*, 1687–1692.
- (17) Lichtenhan, J. D.; Vu, N. Q.; Carter, J. A.; Gilman, J. W.; Feher, F. J. *Macromolecules* **1993**, *26*, 2141–2142.
- (18) Haddad, T. S.; Lichtenhan, J. D. *Macromolecules* **1996**, *29*, 7302–7304.
- (19) Fu, B. X.; Zhang, W. H.; Hsiao, B. S.; Rafailovich, M.; Sokolov, J.; Sauer, B. B.; Phillips, S.; Balski, R. *High Perform. Polym.* **2000**, *12*, 565–571.
- (20) Green, P.; Christensen, T.; Russell, T.; Jerome, R. *Macromolecules* **1989**, *22*, 2189–2194.
- (21) Russell, T. P. *Mater. Sci. Rep.* **1990**, *5*, 171–210.

- (22) Zhu, S.; Liu, Y.; Rafailovich, M. H.; Sokolov, J.; Gersappe, D.; Winesett, D. A.; Ade, H. *Nature* **1999**, *400*, 49–51.
- (23) (a) Lichtenhan, J. D.; Otonari, Y. A.; Carr, M. J. *Macromolecules* **1995**, *28*, 8435–8437. (b) Pyun, J.; Matyjaszewski, K. *Macromolecules* **2000**, *33*, 217–220.
- (24) Jacobsen, C.; Williams, S.; Anderson, E.; Brown, M. T.; Buckley, C. J.; Kern, D.; Kirz, J.; Rivers, M.; Zhang, X. *Opt. Commun.* **1991**, *86*, 351.
- (25) Ade, H.; Urquhart, S. G. *Chemical Applications of Synchrotron Radiation*; World Scientific: Singapore, 2001.
- (26) Sikka, M.; Pellegrini, N. N.; Schmitt, E. A.; Winey, K. I.; *Macromolecules* **1997**, *30*, 445–455.
- (27) Ade, H.; Winesett, D. A.; Smith, A. P.; Qu, S.; Ge, S.; Sokolov, J.; Rafailovich, M. *Europhys. Lett.* **1999**, *45*, 526–532.
- (28) Clarke, C. J.; Eisenberg, A.; Scala, J. L.; Rafailovich, M. H.; Sokolov, J.; Li, Z.; Qu, S.; Nguyen, D.; Schwarz, S. A.; Strzhemechny, Y.; Sauer, B. B. *Macromolecules* **1997**, *30*, 4184–4188.
- (29) Demarquette, N. R.; Kamal, M. R. *Polym. Eng. Sci.* **1994**, *34*, 1823–1833.
- (30) Israels, R.; Jasnow, D.; Balazs, A. C.; Guo, L.; Krausch, G.; Sokolov, J.; Rafailovich, M. *J. Chem. Phys.* **1995**, *102*, 8149–8157.
- (31) Shimizu, R. N.; Demarquette, N. R. *J. Appl. Polym. Sci.* **2000**, *76*, 1831–1845.
- (32) Slep, D.; Asselta, J.; Rafailovich, M. H.; Sokolov, J.; Winesett, D. A.; Smith, A. P.; Ade, H.; Anders, S. *Langmuir* **2000**, *16*, 2369–2375.
- (33) Sferrazza, M.; Xiao, C.; Jones, A. L.; Bucknall, D. G.; Webster, J.; Penfold, J. *Phys. Rev. Lett.* **1997**, *78*, 3693–3696.
- (34) Seeck, O. H.; Kaendler, I. D.; Tolan, M.; Shin, K.; Rafailovich, M. H.; Sokolov, J.; Kolb, R. *Appl. Phys. Lett.* **2000**, *76*, 2713–2715.
- (35) Anastasiadis, S.; Chen, J.; Koberstein, J.; Siegel, A.; Sohn, J.; Emerson, J. *J. Colloid Interface Sci.* **1987**, *119*, 55–66.
- (36) Liu, Y.; Rafailovich, M.; Sokolov, J.; Schwarz, S.; Zhong, X.; Eisenberg, A.; Kramer, E.; Sauer, B.; Satija, S. *Phys. Rev. Lett.* **1994**, *73*, 440–443.

MA020725I